Proceedings World Geothermal Congress 2020+1
Reykjavik, Iceland, April - October 2021

Volcano-Tectonic Structures and Their Influence on Soil Gas Emissions in a Low Permeable Geothermal Reservoir – A Case Study from Los Humeros Volcanic Complex, Mexico

Anna Jentsch[1,2], Egbert Jolie[1], Dave G Jones[3] Helen-Taylor Curran[3], Loïc Peiffer[4], and Martin Zimmer[1]

[1]Helmholtz Centre Potsdam, GFZ German Research Centre For Geosciences, Telegrafenberg, 14473 Potsdam, Germany

[2]Institute of Earth and Environmental Science, University of Potsdam, 14476 Potsdam, Germany

[3]Environmental Science Center, British Geological Survey, Keyworth, NG12 5GG, Nottingham, England, United Kingdom

[4]Departamento de Geología, Centro de Investigación Científica y de Educación Superior de Ensenada (CICESE), Ensenada, Baja California, Mexico

ajentsch@gfz-potsdam.de

Keywords: Scouting survey; soil degassing; CO_2 efflux; carbon and helium isotopes; radon, fault zone analysis; systematic sampling approach

ABSTRACT

The Mexican-European research cooperation GEMex enables to study one of the largest geothermal fields in Mexico, the Los Humeros Volcanic Complex (LHVC). By means of different soil gas techniques, we investigated their applicability to understand the structural pattern and characteristics of the volcanic-geothermal system. The geothermal field is characterized by a low permeable caprock where fluid upflow is mainly controlled by volcano-tectonic structures. We developed an optimal sampling approach and network covering the main production zone of the geothermal field measuring different soil gases in order to understand their spatial variability. CO_2 efflux measurements were performed by the accumulation chamber technique and elevated emissions were measured along known faults as well as in areas of unknown fault related permeability. This was complemented by alpha spectroscopy for ^{222}Rn and ^{220}Rn emissions as well as soil temperature measurements at 50 cm depth. The results show a positive correlation with CO_2 efflux although in a few areas different behavior was observed for soil temperatures and ^{222}Rn concentrations.

Additional work focused on the origin of geothermal gases. $\delta^{13}C$ analyses of degassing CO_2 and $^3He/^4He$ ratios can be a useful tool for the differentiation of the source of gas. $\delta^{13}C$ results give evidence for a magmatic system with some contribution from the meta carbonates composing the basement. Elevated $^3He/^4He$ ratios indicate a mantle contribution in areas of anomalous CO_2 and ^{222}Rn degassing.

Our results suggest that especially the combination of different soil gas measurements is a useful approach to indicate structural discontinuities in the subsurface that act as migration pathways of hydrothermal fluids. Some of the highest values from the investigated parameters were measured in areas of unknown structural permeability. Furthermore, we would like to point out that a strategic sampling network plays a major role not only to identify but also to determine the geometry and distribution of the most permeable parts along volcano-tectonic structures.

1. INTRODUCTION

Volcanic-hosted geothermal systems comprise a vast amount of thermal energy where reservoir fluids can reach supercritical conditions linked to magmatic intrusions. The supercritical state of a fluid is defined for pure water at T > 374 °C and P > 221 bar (Heřmanská et al., 2019). The assessment, characterization, and development of a so called super-hot geothermal resource is the focus of the Mexican-European research cooperation GEMex studying the Los Humeros Volcanic Complex (LHVC). The main control for fluid upflow in the reservoir is given by volcano-tectonic structures (e.g. faults and magmatic intrusions) which cut through the low permeable pre-caldera Teziutlán formation (Gutiérrez-Negrín and Izquierdo-Montalvo, 2010). In this study, we present the results of a systematic, large scale CO_2 efflux scouting survey in order to understand the spatial variability of CO_2 degassing and the relation to possible migration pathways of hydrothermal fluids reaching the surface. From all volcanic gases, CO_2 is the most abundant one and is a particularly useful parameter for soil gas measurements as it exsolves from magma at greater depth and has an elementary importance in geothermal-volcanic systems (Edmonds and Wallace, 2017). CO_2 effluxes were complemented by the sampling of carbon and helium isotopes from selected sites. By means of carbon isotopic analysis the origin and different processes, affecting the migration of CO_2 can be identified. Helium isotopic ratios ($^3He/^4He$) are excellent tracer for deep derived fluids since ^3He is primordial released by the mantle (Karlstrom et al., 2013; Notsu et al., 2001). The spatial distribution of elevated ^{222}Rn (radon) and ^{220}Rn (thoron) emissions in geothermal and volcanic settings can be related to faults/fractures that act as preferential pathways to the ascent of radon gas from depth or might be related to intense rock fracturing (Giammanco et al., 2007; Hernández et al., 2004). Radon and thoron are the only radioactive gases being chemically inert and continuously generated by the ^{238}U and ^{232}Th decay series. Because of the different half-lives of radon (3.8 days) and thoron (55 seconds), the $^{222}Rn/^{220}Rn$ ratio can be used to discuss the origin of possible deep or shallow derived radon gas. Based on the CO_2 efflux results of the large scale scouting survey, four areas of increased CO_2 emissions were selected and grid spacing was refined to gain a higher resolution of the extent of increased degassing areas and relate them to the structural architecture of fault zones. In this way, the exact location of permeable segments along and within fault zones can be determined and supports the identification of possible drilling targets.

2. STUDY AREA

The Los Humeros Volcanic Complex is located at the eastern portion of the Trans-Mexican Volcanic Belt (TMVB) being the largest, active, silicic caldera complex in Mexico and hosting a geothermal field with an installed capacity of 95 MW (Fig. 1a) (Gutiérrez-Negrín, 2019). The caldera has a complex geological and structural history and its evolution started around 164 ± 4.2 ka ago resulting in the 20 km wide Los Humeros trap-door caldera. The activity continued with a series of plinian eruptions and was followed by a second caldera forming event at around 69 ± 16 ka ago leaving the semicircular Los Potreros caldera which hosts the active geothermal system. The post-caldera stage is characterized by changing episodes of effusive and explosive eruptions many of them of monogenetic origin lasting until the Holocene (Carrasco-Núñez et al., 2017). The main fault system at Los Humeros is marked by a slightly curvilinear NNW-SSE fault system consisting of Los Humeros and Maztaloya Fault as well as some N-S oriented sub-parallel smaller faults and fault splays (La Cuesta, Loma Blanca etc.) (Fig. 1b), which induce and preserve the permeability of the geothermal system associated with the active resurgence of the LHVC. Besides that, there are several faults with a NE-SW and E-W orientation revealing the complexity of the deformation pattern resulting from compressive and extensional phases during caldera formation (Norini et al., 2015). This is supported by the isotopic fingerprint of geothermal fluids, which shows a mixing between andesitic and meteoric waters. The complex fault and fracture network cuts through the abundant volcanic succession of syn- and post-caldera units and allows meteoric water to infiltrate into the geothermal reservoir (Gutiérrez-Negrín and Izquierdo-Montalvo, 2010). Volcano-tectonic deformation along faults at Los Humeros is dated by ^{14}C radiometry on a displaced paleosol to 7.3 ± 0.1 ka overlain by pyroclastic fall deposits (Cuicuiltic Member) (Dávila-Harris and Carrasco-Núñez, 2014; Norini et al., 2015). This is an evidence for the young structural activity inside the caldera. Furthermore, many of the faults located inside the main production zone show extensive fossil and active hydrothermal alteration.

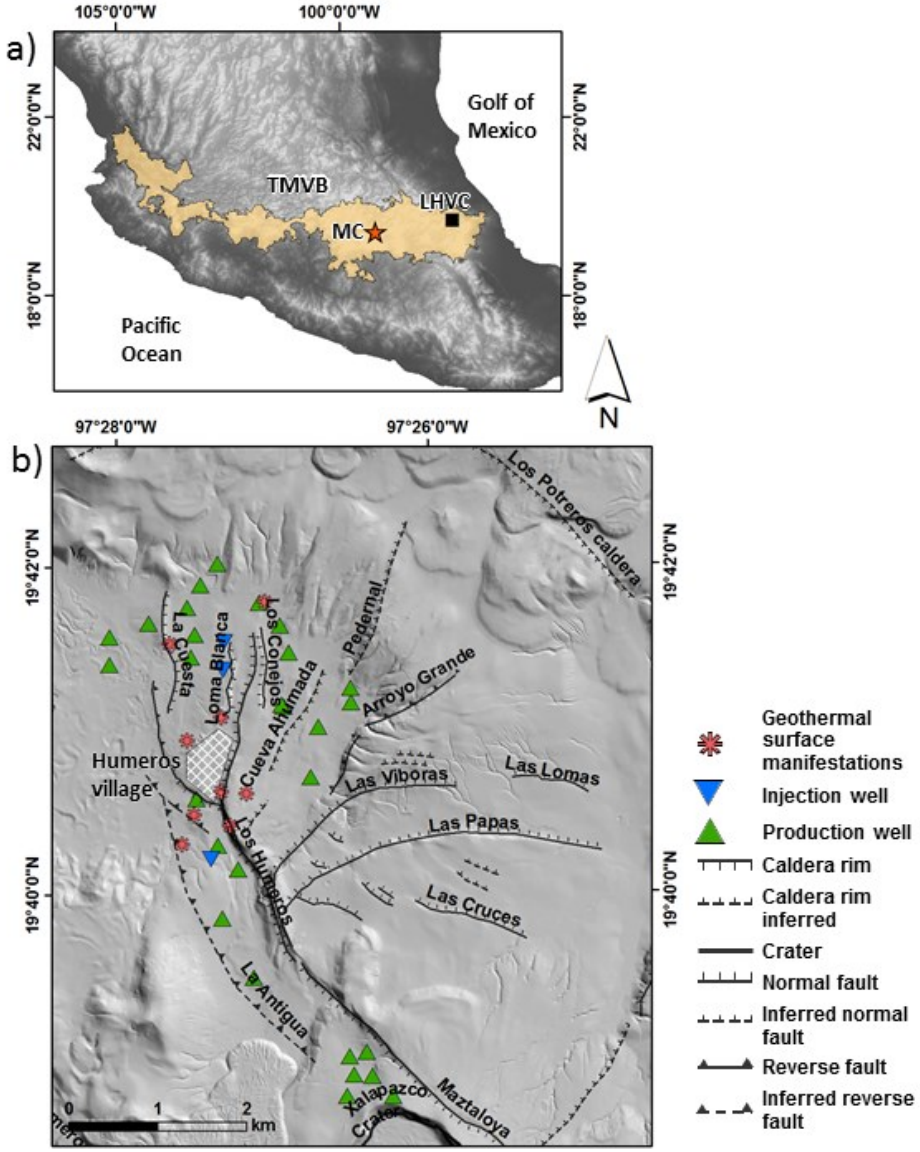

Figure 1: a) Map showing the central part of Mexico and the location of the Los Humeros volcanic complex (LHVC) within the Trans Mexican Volcanic Belt (TMVB). MC: Mexico City b) High resolution digital elevation model (1m) from Carrasco-Núñez et al., (2017) of the study area showing all injection and production wells. Solid and dashed black lines represent volcano-tectonic structures resumed from Norini et al., (2019) with nomenclature. Red asterisks show locations of geothermal surface manifestations e.g. advanced argillic alteration, weak steam vents, sulphur deposits, and hot ground, which were identified during the survey.

3. METHODS AND RESULTS

3.1 Sampling approach

For the first survey, we developed a regular, large-scale sampling network consisting of 2700 CO_2 efflux sampling points with the objective to investigate the entire geothermal field to detect spatial variabilities of soil degassing. This allowed us to scout all areas in the main production zone for a later refinement of the sampling network in particular areas. The sampling network was defined by a 25 × 200 m spacing where the short spacing was always oriented perpendicular to the major fault strike (Table 1). Based on the results of the first CO_2 efflux scouting survey, three areas of interest with elevated CO_2 emissions were selected. These areas (Area A, D, and E) were investigated in more detail during a second CO_2 efflux survey. Through the small-scale surveys we achieved a higher resolution of the extent of elevated degassing and could show their heterogeneity over short distances. This helps to understand the internal fault structure which shows different degassing behavior along its damage zone (Caine et al., 1996; Jolie et al., 2016) and the most permeable segments of the faults. In total 798 sampling points were measured with a variable point distance while profile distance was refined to 100 m except for Area D, where a very fine sampling grid of 10 x 10 m was applied. The measurement of ^{222}Rn and ^{220}Rn emissions and soil temperatures were performed at the same sampling sites as CO_2 efflux with a reduction in its point distance to every 50 m due to longer measurement time.

3.2 Methods

Herein, all measurements of soil CO_2 efflux were performed with a portable LICOR LI-820 infrared gas analyzer from West Systems which is connected through a closed loop to an accumulation chamber (West Systems Ltd, 2019). A detailed description about the accumulation chamber method can be found in Chiodini et al., (1998). Additionally, soil temperatures were measured in 50 cm depth with a Greisinger GMH 285-BNC thermometer coupled to a Pt1000 sensor and a 620 mm long stainless steel probe (accuracy ±0.1 K). For the identification of the origin of CO_2, a total of 94 soil gas samples were collected from low, intermediate and high degassing areas for $\delta^{13}C_{CO_2}$ isotopic ratios analysis. Isotopic determinations were performed with a Delta V Plus gas chromatograph coupled to an isotopic ratio mass spectrometer. To further constrain the origin of soil gases, six helium samples from weak to moderate steam vents were taken to determine the $^3He/^4He$ ratios. The samples were analyzed with a Helix SFT mass spectrometer and are normalized to the air ratio ($R/R_A = 1.386 \times 10^{-6}$). By means of a portable Sarad RTM2200 monitor, the radon (^{222}Rn) and thoron (^{220}Rn) activity concentration in soil gas samples were determined by radiometric in-situ measurements of their short-living daughter products (^{218}Po and ^{216}Po,respectively) emitting alpha radiation at nuclide specific energies. In comparison with CO_2 efflux measurements, which are performed at the soil-atmosphere interface, radon (^{222}Rn) and thoron (^{220}Rn) activity concentration measurements are conducted in 1 m depth by inserting a metal probe into the ground. As the small village (Humeros) is much affected by man-made disturbances we did not perform any CO_2 efflux measurements there, whereas radon/thoron activity concentration measurements are unaffected and complement the dataset in this area. In order to understand the spatial variability of investigated parameters a series of CO_2 efflux, and soil temperature interpolation maps were generated by means of Sequential Gaussian Simulations (sGs) based on a simple kriging model using ESRI ArcGIS 10.5 software.

3.3 Results

CO_2 efflux values show a wide range and vary from 0 to 1,464.2 g m^{-2} d^{-1} (Table 1). By applying the graphical statistical analysis on the total dataset two inflection points where identified which divide the dataset into three populations. Population A corresponds to low 'background' effluxes (0.1 – 20. 7 g m^{-2} d^{-1}). Population B is a mixed population showing the widest range of values (20.7 – 640.8 g m^{-2} d^{-1}), and population C includes the highest measured values (670.8 – 1464.2 g m^{-2} d^{-1}). Zones exceeding the background thresholds (Area A to F) occur over the entire study area (Fig. 2a). Results for carbon isotopic analysis of CO_2 range from -23.2 ‰ to -1.2 ‰ ± 0.07 ‰ covering a broad spectrum of sources. Carbon isotopic compositions characterized by a hydrothermal signature (-1.8 to -6.3 ‰) coincide with increased CO_2 degassing areas (Fig. 2). Soil temperatures in 50 cm depth vary from 5.7 to 91.3 °C. Most thermal anomalies appear in areas of elevated degassing (Area A-E) with two exceptions (Area J & K; Fig. 3). The highest temperature of 91.3 °C occurs together with sulphur deposits and a weak steam vent in Area C. The measured $^3He/^4He$ ratios range from 2.31 ± 0.58 to 4.88 ± 0.99 and deviate from the typical air helium isotopic ratio ($R_A = 1.386$ x 10-6) showing a mantle contribution. The two highest $^3He/^4He$ ratios correlate with the two maximum measured CO_2 effluxes located in Area A and E (Fig. 2 & 3). Values for radon (^{222}Rn) and thoron (^{220}Rn) activity concentrations vary from 110 to 100727 Bq/m³ and 135 to 35063 Bq/m³, respectively (Table 1). The spatial variation of elevated radon concentrations (>13000 Bq/m³) shows similar patterns to that of CO_2 efflux.

Table 1: Summary of all measured parameters and sampling specifications. VPBD = Vienna Pee Dee Belemnite

Parameters	Size of study area [km]	Grid spacing [m]	N°	Min	Max	Mean
CO_2 efflux [g $m^{-2}d^{-1}$]	6 × 4	25 × 200 25 × 100	3500	0	1464.2	8.5
$\delta^{13}C$-CO_2 [δ ‰ vs. VPBD]	Selected sites	Single points	74	-23.2	-1.2	-7.9
T_s [°C]	5.8 × 2.4	50 × 200	858	5.9	91.3	17.5
$^3He/^4He$ [R/R_a]	Selected sites	Single points	6	2.31	4.88	3.4
^{222}Rn/ ^{220}Rn [Bq m^{-3}]	5.8 × 2.4	50 × 200	858	110/ 135	100700/ 35063	3600/ 3830

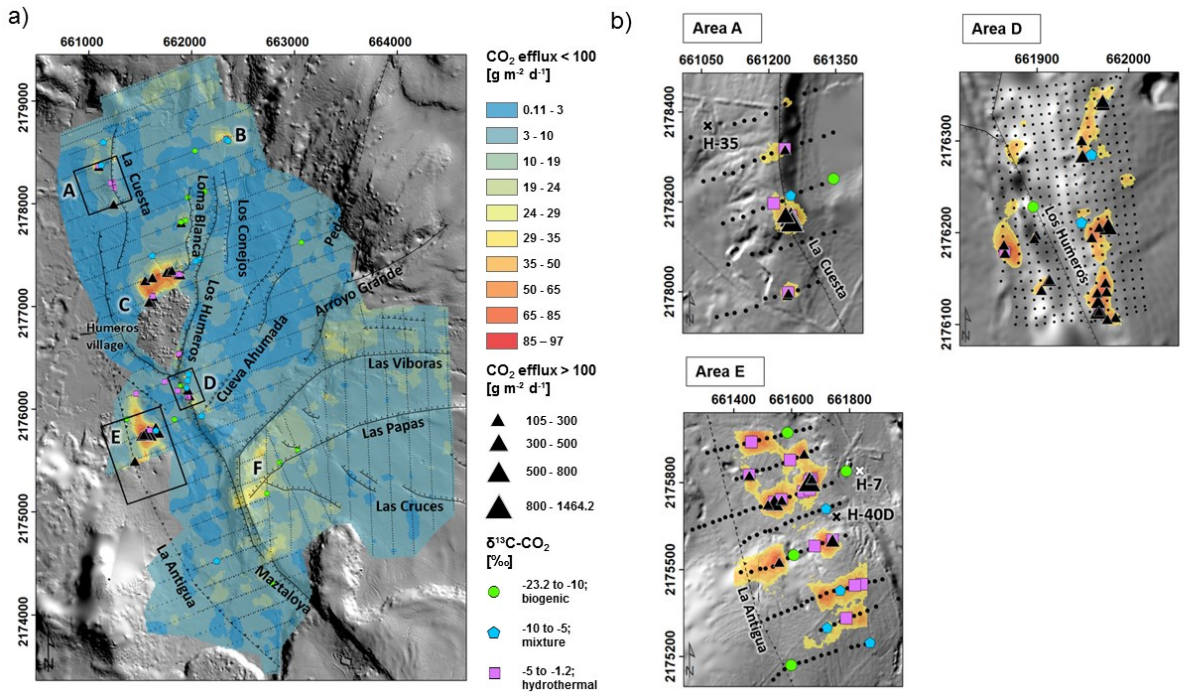

Figure 2: a) Results of sequential Gaussian simulation for CO_2 efflux measurements showing the distribution of low, intermediate and increased degassing sites until 100 g m^{-2} d^{-1}. Bold capital letters refer to areas explained in the chapters results and discussion. Black squares show the location and size of the small-scale surveys. b) CO_2 efflux maps for Area A, D, and E. Values lower than 29 g m^{-2} d^{-1}are masked. Black crosses show location of production wells. The white cross in Area E shows an injection well. Graduated black triangles show CO_2 efflux values above 100 g m^{-2} d^{-1}. Carbon isotopes (green circle, blue pentagon, and purple square) are classified in three groups depending on their source. Small black dots represent CO_2 efflux sampling sites. Solid and dashed black lines with names show known and inferred faults.

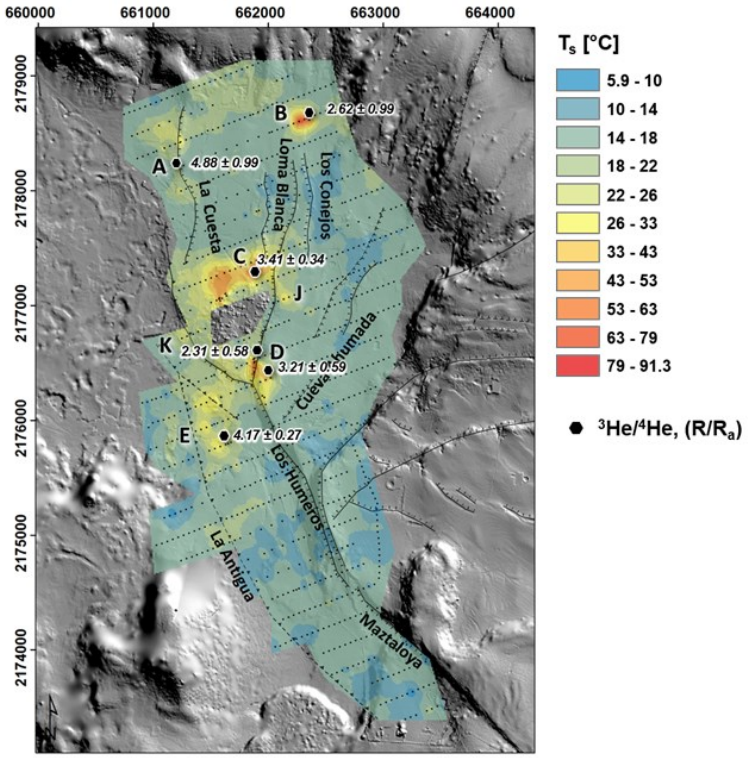

Figure 3: Results of sequential Gaussian simulation for measured soil temperatures. Black small dots represent soil temperature sampling sites. Black hexagons show sampling sites and results for air corrected helium ratio measurements at weak to moderate steam vents. Bold capital letters refer to the text. Solid and dashed black lines show known and inferred faults with nomenclature.

4. DISCUSSION

4.1 CO_2 efflux populations and origin of CO_2 based on $\delta^{13}C_{CO_2}$ isotopic ratio analysis

The majority of measured CO_2 efflux values belongs to the background population (0 – 20.7 g m^{-2} d^{-1}). As shown for other active caldera complexes worldwide (Peiffer et al., 2014, 2018; Werner et al., 2000), these low fluxes typically originate from biogenic degassing (i.e. soil respiration and organic decomposition). Additionally, most $\delta^{13}C$ analysis of soil CO_2 acquired in this study confirms this hypothesis ($\delta^{13}C$ < -10 ‰). However, five samples with an efflux value lower than 20.7 g m^{-2} d^{-1} have $\delta^{13}C_{CO2}$ isotopic compositions ranging from -3.9 ‰ to --7 ‰, indicating a clear contribution of hydrothermal/ mantle CO_2. Peiffer et al. (2014) report that CO_2 of hydrothermal origin can be transported by advection at low rates, similar to biogenic degassing rates, due to a low-permeability of soils/rocks and/or low-pressure gradients. Furthermore, these values appear in the vicinity of elevated CO_2 degassing areas (< 200 m away) and show that the actual size of a structural discontinuity/ zone of enhanced permeability can extent further to what is observed by solely analyzing CO_2 effluxes. The relatively large range of effluxes in population B (20 - 669 g m^{-2} d^{-1}) results from combined CO_2 sources as well as transport mechanisms. Corresponding $\delta^{13}C_{CO2}$ values range from -18 ‰ up to -1.2 ‰. This constrains that CO_2 emissions are a result of biologic and volcanic degassing driven by diffusive and advective transport mechanisms. Population C (640 – 1468 g m^{-2} d^{-1}) is characterized by more heavy $\delta^{13}C_{CO2}$ values (-4 to -3 ‰), which typically indicate a hydrothermal source. Carbon isotopic analyses revealed that almost all areas of elevated CO_2 emissions (Area A, B, C, D, E) show $\delta^{13}C_{CO2}$ values with a mantle/hydrothermal signature. Eventually we could show that the separation of CO_2 effluxes by only using the GSA method is not significant enough in order to distinguish between biogenic and hydrothermal soil degassing.

4.2 Soil degassing and its relationship to fault zone architecture

It is from great importance to not only understand the loci of faults/fault zones instead we also need to determine the most active and permeable fault segments. CO_2 and ^{222}Rn degassing is typically not limited to a single fault plane instead it is influenced by wide fault zones of anisotropic and heterogeneous characteristics along its strike. Faulds and Hinz, (2015) defined different structural settings in the Basin and Range Province which favor the development for geothermal systems. This general classification can be applied to other geothermal systems and is brought in to context with our results. Increased CO_2 emissions in Area A and D are following the known La Cuesta and Los Humeros normal faults, while degassing also extends into their foot- and hanging walls (Fig. 2b). Apparently, degassing along Los Humeros fault is restricted to a 680 m long NNW-SSE sector pointing to the most permeable part of this major normal fault with a connection to the deep geothermal system. This can be explained by an impermeable fault core due to intense hydrothermal alteration supported by reddish brown colors and increased surface temperatures on its fault scarp. The largest and unknown degassing corridor, related to hydrothermal carbon and helium isotopes with a contribution of the mantle, appears in Area E reaching 350 m E-W and 900 m N-S extension. The size and pattern of degassing follows the typical NNW-SSE orientation of faults in Los Humeros and might either be a result of a fault intersection or an accommodation zone comprising multiple faults linking in the subsurface. This corresponds to long-term, critically stressed areas where fluid pathways tend to remain open (Faulds and Hinz, 2015). Area C is pronounced by a 550 m E-W corridor north of Los Humeros village and extends about 250 m in N-S direction. The appearance of increased emissions differs from the main structural trend and gives indication for a more complex and hidden structural setting. It can be the result of a horsetail fault termination starting south of Humeros village. Los Humeros represents the range front fault with multiple, asymmetrically arranged faults spreading off and forming a horsetail towards the north. This configuration promotes the uprising of hot fluids as seen by hot surface temperatures (91.3°C), sulphur deposits, mantle derived helium and hydrothermal carbon. Additionally, ^{222}Rn measurements which were performed in the village give evidence for this interpretation due to increased concentrations. A positive correlation between CO_2 effluxes and ^{222}Rn concentrations can be seen in figure 4 especially in areas characterized by anomalous degassing. An inverse relationship between $^{220}Rn/^{222}Rn$ ratio and CO_2 efflux is the result of an excess of ^{222}Rn, which lowers the ratio and allows us to differentiate between deep derived soil gases or shallow. A low ratio suggests deep degassing whereas high ratios indicate shallow ^{222}Rn and ^{220}Rn sources from soil/rock (Giammanco et al., 2007).

5. CONCLUSION

We here present results of a comprehensive large-scale soil gas survey at Los Humeros geothermal field where we identified new areas (Area C and E) of increased permeability related to structural discontinuities in the subsurface of the main geothermal production zone. Degassing at Los Humeros geothermal field is primarily controlled by an abundant fault network, which is partly buried and has a connection to the deep geothermal system. Our findings show that the majority of increased CO_2 emissions at the surface is hydrothermally derived CO_2 migrated along deep reaching faults and fractures from the reservoir. This is confirmed by the location of most of the production wells drilled along the known active fault system. Carbon and helium isotopic analysis provide crucial evidence for the relationship of elevated soil gases connected to the deep geothermal reservoir. Furthermore, results of carbon isotopic analyses showed that the application of determined $\delta^{13}C_{CO_2}$ groups is an additional tool to delineate areas of deep derived CO_2 than solely using CO_2 effluxes. The appearance of elevated ^{222}Rn emissions shows mostly a good correlation to CO_2 effluxes with the addition that the measurements of ^{222}Rn and ^{220}Rn emissions are not limited by man-made disturbances like the village. Regular large-scale surveys can be used for scouting purposes especially in areas with little information about the subsurface geology. We encourage the application of soil gas studies for resource assessment in new and undeveloped geothermal sites and its use for the localization of potential drilling targets in combination with other scientific disciplines e.g. structural geology, geophysics, remote sensing. Within the term of the GeMEX project a substantial database is compiled which enables to confirm some of our findings.

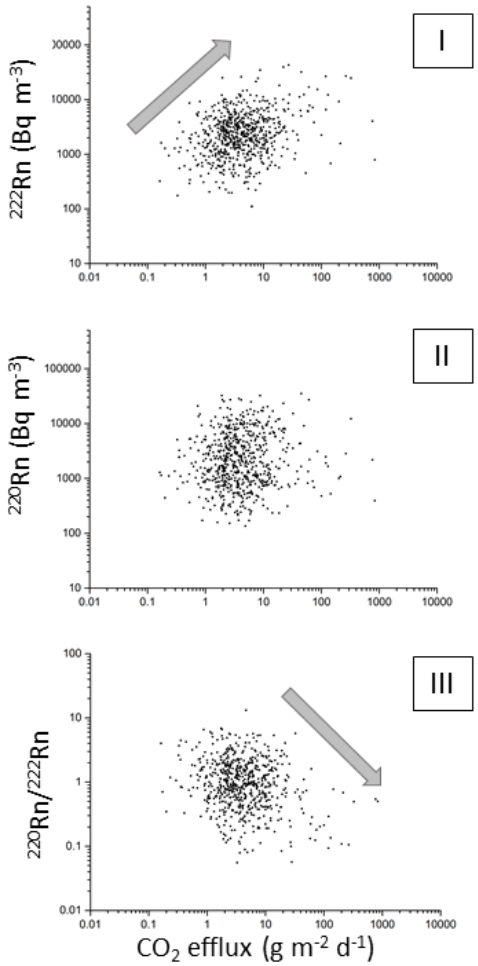

Figure 4: Correlation between CO_2 efflux and I: ^{222}Rn, II: ^{220}Rn, III: ^{220}Rn/^{222}Rn. Grey arrows indicate a I: positive and III: Inverse correlation between the investigated parameters.

6. ACKNOWLEDGEMENTS

This paper presents results of the GEMex Project, funded by the European Union's Horizon 2020 research and innovation programme under Grant Agreement No.727550, and by the Mexican Energy Sustainability Fund CONACYT-SENER, Project2015-04-268074. The authors wish to thank the Comisión Federal de Electricidad of Mexico (CFE) for their support, and access to Los Humeros geothermal field. A special thank you to all people from Mexico, Argentina, and Germany who supported us to collect this comprehensive dataset: Esteban Silva, Sonia Vargas Pineda, Romel González, Ana Maria Dávalos Pérez, Jorge Alejandro Guevara Alday, Ruth Alfaro Cuevas Villanueva, Rojeh Khleif, Tanja Ballerstedt, Camila Espinoza, Leandra Weydt, and Adrian Lechel. Thank you to the GEMex consortium but especially to Gianluca Norini for fruitful discussions. Thank you to the Universidad Michoacana de San Nicolás de Hidalgo for providing vehicles for the fieldwork.

REFERENCES

Caine, J.S., Evans, J.P., Forster, C.B. (1996). Fault zone architecture and permeability structure. Geology 24, 1025–1028.

Carrasco-Núñez, G., Hernández, J., De León, L., Dávila-Harris, P., Norini, G., Bernal, J.P., Jicha, B., Navarro, M., López-Quiroz, P. (2017). Geologic Map of Los Humeros volcanic complex and geothermal field, eastern Trans-Mexican Volcanic Belt Mapa geológico del complejo volcánico Los Humeros y campo geotérmico, sector oriental del Cinturón Volcánico Trans-Mexicano. Terra Digitalis 1, 1–11. https://doi.org/10.22201/igg.terradigitalis.2017.2.24.78

Chiodini, G., Cioni, R., Guidi, M., Raco, B., Marini, L. (1998). Soil CO2 flux measurements in volcanic and geothermal areas. Applied Geochemistry 13, 543–552. https://doi.org/10.1016/S0883-2927(97)00076-0

Dávila-Harris, P., Carrasco-Núñez, G. (2014). An unusual syn-eruptive bimodal eruption: The Holocene Cuicuiltic Member at Los Humeros caldera, Mexico. Journal of Volcanology and Geothermal Research. https://doi.org/10.1016/j.jvolgeores.2013.11.020

Edmonds, M., Wallace, P.J. (2017). Volatiles and exsolved vapor in volcanic systems. Elements 13, 29–34. https://doi.org/10.2113/gselements.13.1.29

Faulds, J.E., Hinz, N.H. (2015). Favorable Tectonic and Structural Settings of Geothermal Systems in the Great Basin Region , Western USA: Proxies for Discovering Blind Geothermal Systems. World Geothermal Congress 2015 1–6.

Giammanco, S., Sims, K.W.W., Neri, M., (2007). Measurements of 220 Rn and 222 Rn and CO2 emissions in soil and fumarole gases on Mt. Etna volcano (Italy): Implications for gas transport and shallow ground fracture. Geochemistry, Geopysics, Geosystems 8, 1–14. https://doi.org/10.1029/2007GC001644

Gutiérrez-Negrín, L.C.A., (2019). Current status of geothermal-electric production in Mexico Current status of geothermal-electric production in Mexico, in: IOP Conf. Series: Earth and Environmental Science 249 (012017). https://doi.org/10.1088/1755-1315/249/1/012017

Gutiérrez-Negrín, L.C.A., Izquierdo-Montalvo, G., (2010). Review and Update of the Main Features of the Los Humeros Geothermal Field, Mexico, in: World Geothermal Congress 2010. https://doi.org/10.1016/j.bmc.2011.02.011

Heřmanská, M., Kleine, B.I., Stefánsson, A., (2019). Supercritical Fluid Geochemistry in Geothermal Systems. Geofluids 2019, 1–14. https://doi.org/10.1155/2019/6023534

Hernández, P., Pérez, N., Salazar, J., Reimer, M., Notsu, K., Wakita, H., (2004). Radon and helium in soil gases at Cañadas caldera, Tenerife, Canary Islands, Spain. Journal of Volcanology and Geothermal Research 131, 59–76. https://doi.org/10.1016/S0377-0273(03)00316-0

Jolie, E., Klinkmueller, M., Moeck, I., Bruhn, D., (2016). Linking gas fluxes at Earth's surface with fracture zones in an active geothermal field. Geology 44, 187–190. https://doi.org/10.1130/G37412.1

Karlstrom, K.E., Crossey, L.J., Hilton, D.R., Barry, P.H., (2013). Mantle 3He and CO2 degassing in carbonic and geothermal springs of Colorado and implications for neotectonics of the Rocky Mountains. Geology 41, 495–498. https://doi.org/10.1130/G34007.1

Norini, G., Carrasco-Núñez, G., Corbo-Camargo, F., Lermo, J., Hernández Rojas, J., Castro, C., Bonini, M., Montanari, D., Corti, G., Moratti, G., Piccardi, L., Chavez, G., Zuluaga, M.C., Ramirez, M., Cedillo, F., (2019). The structural architecture of the Los Humeros volcanic complex and geothermal field. Journal of Volcanology and Geothermal Research 118, 17–26. https://doi.org/https://doi.org/10.1016/j.marpolbul.2017.02.048

Norini, G., Groppelli, G., Sulpizio, R., Carrasco-Núñez, G., Dávila-Harris, P., Pellicioli, C., Zucca, F., De Franco, R., (2015). Structural analysis and thermal remote sensing of the Los Humeros Volcanic Complex: Implications for volcano structure and geothermal exploration. Journal of Volcanology and Geothermal Research 301, 221–237. https://doi.org/10.1016/j.jvolgeores.2015.05.014

Notsu, K., Nakai, S., Igarashi, G., Ishibashi, J., Mori, T., Suzuki, M., Wakita, H., (2001). Spatial distribution and temporal variation of 3 He / 4 He in hot spring gas released from Unzen volcanic area , Japan. Journal of Volcanology and Geothermal Research 111, 89–98.

Ozima, M. and Podosek, F.A., (2002). Noble gas geochemistry., 2nd ed. Cambridge University Press.

Peiffer, L., Bernard-Romero, R., Mazot, A., Taran, Y.A., Guevara, M., Santoyo, E., (2014). Fluid geochemistry and soil gas fluxes (CO2-CH4-H2S) at a promissory Hot Dry Rock Geothermal System: The Acoculco caldera, Mexico. Journal of Volcanology and Geothermal Research 284, 122–137. https://doi.org/10.1016/j.jvolgeores.2014.07.019

Peiffer, L., Carrasco-Núñez, G., Mazot, A., Villanueva-Estrada, R.E., Inguaggiato, C., Bernard Romero, R., Rocha Miller, R., Hernández Rojas, J., (2018). Soil degassing at the Los Humeros geothermal field (Mexico). Journal of Volcanology and Geothermal Research 356, 163–174. https://doi.org/10.1016/j.jvolgeores.2018.03.001

Werner, C., Brantley, S.L., Boomer, K., (2000). CO2 emissions related to the Yellowstone volcanic system 2. Statistical sampling, total degassing, and transport mechanisms. Journal of Geophysical Research 105, 10,831-10,846.

West Systems Ltd, W., (2019). Portable diffuse flux meter WEST Systems, Handbook, Release 9.1.